Out-of-plane STM displacement measurements and evaluation of elastic fields in iron silicide islands on silicon

Y. Manassen,[1] H. Realpe,[1] R. Shneck,[2] D. Barlam,[3] and A. Brokman[4]
[1]*Department of Physics and the Ilse Katz Center for Nonometer Scale Science and Technology, Ben Gurion University, P.O. Box 653, Beer Sheva 84105, Israel*
[2]*Department of Materials Engineering, Ben Gurion University, P.O. Box 653, Beer Sheva 84105, Israel*
[3]*Department of Mechanical Engineering, Ben Gurion University, P.O. Box 653, Beer Sheva 84105, Israel*
[4]*School of Applied Science, Hebrew University of Jerusalem, Givat Ram, Jerusalem 91904, Israel*
(Received 9 October 2002; published 22 August 2003)

Elastic deformations have been discerned with β-$FeSi_2$ islands grown on Si(111)7×7 by STM. Anisotropic mismatch between the β-$FeSi_2$ and the surface is -5.3% and $+1.4\%$ along $FeSi_2[10\bar{1}]\|Si[\bar{1}\bar{1}2]$ and $FeSi_2[010]\|Si[\bar{1}10]$ respectively. STM images of these islands show threefold symmetry and significant deformations of the surface (the normal to the surface deviates by several degrees from the average substrate normal), both on the islands and around them. Larger islands exhibit smaller deformation, and when deposited on a surface step the island normal tilts towards the upper terrace. Using finite element method in the framework of linear elasticity, the deformations of small islands were simulated, taking into consideration the surface stress. Best agreement with the experimental deformation is obtained when the islands are made of three domains rotated by 120° with respect to each other. The calculations of the deformation agree qualitatively with the measured displacements, and reproduce the deviation of the surface normal. The quantitative difference between the elastic theory and the experimental results may be utilized to gain additional information about the mechanical properties at the surface in the nm scale. The measured deformation of the island also enabled the calculation of the long-range stress fields it generates.

DOI: 10.1103/PhysRevB.68.075412 PACS number(s): 61.46.+w, 07.79.Cz, 46.25.−y

INTRODUCTION

During the last 20 years the theory of elasticity has been invoked to understand various phenomena on the microscale level in surface science,[1–4] primarily as a result of the central role of elastic interactions in the formation and self-ordering of stress relief driven nanostructures like quantum dots[5] or in surface reconstruction.[6] These questions have an increasing technological importance in the field of nanofabrication because of the necessity to assemble several different materials in a small space.

Unfortunately, the small scales involved, made the direct measurements of the elastic fields difficult. Several approaches have been proposed to measure the *average* elastic properties of surfaces. These methods range from measuring the change in phonon spectrum of solids as a result of stress to the bending of a thin cantilever as a result of the stress accumulated at the surface.[6] These methods were used to measure the change in surface stress as a result of adsorption of atoms, growth of epitaxial layers, and structural changes in the surface itself. The effect of *local* strain was used in order to image the surface[7] by means of ultrasonic force microscopy, but other sources of contrast prevent the use of this method for the quantitive measurement of the local stress. To our knowledge (see brief review in the Discussion), there is no method to quantify the local elastic fields, a problem that by and large hindered our progress in understanding surface interactions. The present result demonstrates that together with numerical analysis of the linear equations, it is possible to evaluate the elastic field by means of scanning tunneling microscopy (STM) measurements of the displacements out of the surface plane.

In this work we study the formation of iron silicide islands on the Si(111) 7×7 surface. Several STM studies were performed on iron silicides, epitaxially grown on silicon surfaces.[8–10] In the bulk, the most stable silicide is β-$FeSi_2$. The structure of β-$FeSi_2$ is orthorhombic with the lattice parameters: $a=0.986$ nm, $b=0.779$ nm, $c=0.783$ nm. Despite its stability, it is difficult to grow β-$FeSi_2$ on Si(111) because of a large lattice mismatch [Fig. 1(c)] with the substrate. In general, and without particular treatment, this phase occurs in small islands that transform to the more stable γ-$FeSi_2$ closely packed phase with less than 1% mismatch to the Si(111) surface.

Using STM, it was possible to identify local displacements out of the substrate plan, both in the islands and around them resulting from the misfit between the silicide and the silicon substrate. By employing the finite element method (FEM) to solve the elastic problem (utilizing the misfit strain and surface stress), we found that the elastic deformations explain the fundamental features of the observed displacements. Hence the evaluation of the strain field was made possible by the comparison between the STM measured (out of plan) displacements and the full elastic calculation of the displacements field in the island/substrate system. In general, besides the present application, the result demonstrates qualitatively that profiling the elastic fields around a nanostructure features is possible by means of STM measurements accompanied by numerical elastic calculations.

EXPERIMENTAL PROCEDURE AND RESULTS

The experiment was performed with a custom-made UHV STM with a manual approach mechanism. A silicon wafer

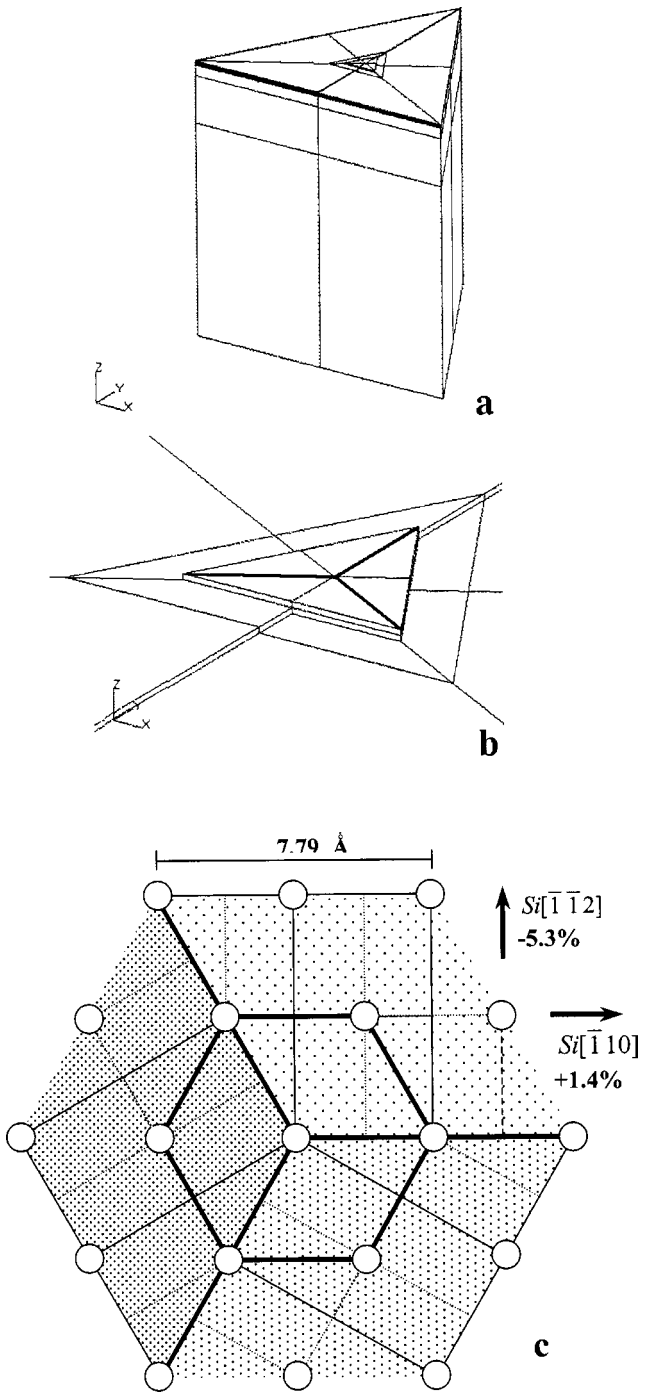

FIG. 1. (a) The finite element model used to simulate the deformation of the island. (b) The finite element model of an island adjacent to a surface step. (c) Schematic drawing of the crystallographic relation between β-$FeSi_2$(101) and Si(111). The three equivalent orientations of the rectangular unit cell of the silicide are drawn.

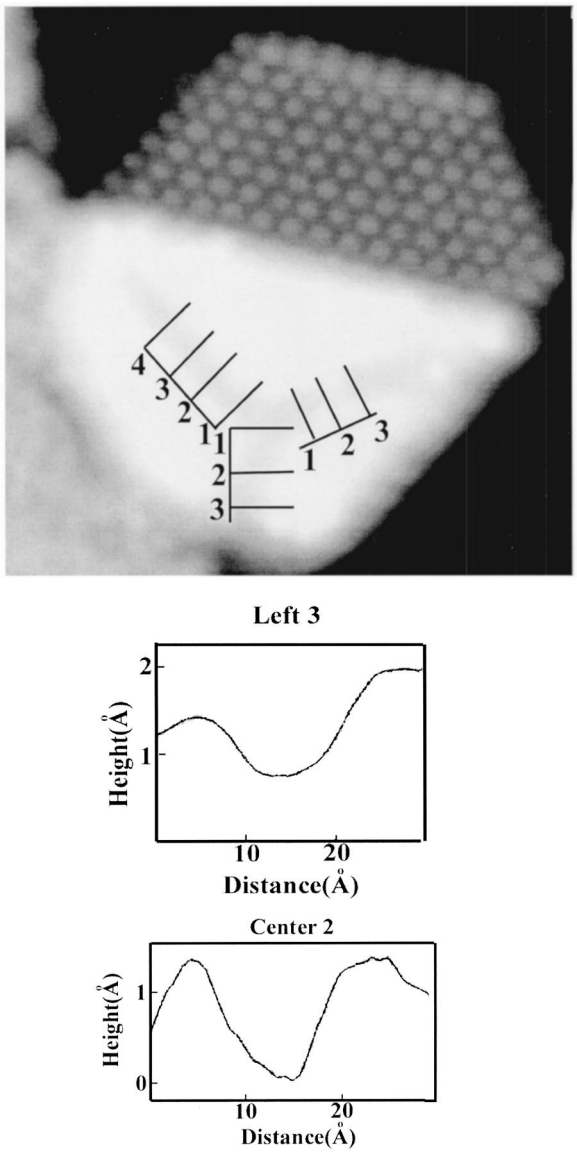

FIG. 2. STM image of a Si(111) 7×7 surface with epitaxial silicide islands on top of it. Part of the island in the center is β-$FeSi_2$ (the lower part) and part of it is γ-$FeSi_2$. The image size is 19 nm^2. Two line scans through the trenches are shown under the image. The image was taken at a bias voltage (V_b) of 2 V and a tunneling current (I_t) of 1 nA.

with a (111) orientation was put in the UHV chamber, after rinsing with several organic solvents (trichloroethylene, acetone, methanol, and dionized water, in this order). After prolonged heating at 900 °C, the sample was heated to 1200 °C for 1 second to decompose the oxide and to induce the 7×7 reconstruction. Low-energy electron diffraction verified that five to ten such flashes are sufficient to induce the reconstruction. Variable amounts of Fe (from 0.05 to 5 monolayers—the amounts were measured with a quartz crystal monitor and verified with STM images before heating) were deposited on the clean surface. Annealing for 3 minutes at a temperature of 450 °C gave a surface that was covered by iron silicide islands having diameters in the range of 3.5–100 nm. STM imaging was done at a positive sample bias of 2 V and a current of 1 nA. Tungsten tips were used. The surface in between the islands is either a perfect or a partially disordered 7×7 structure. Most of the islands have a 2×2 reconstruction that can be easily identified as the γ-$FeSi_2$ phase. The island in Fig. 2 is special in that it is made of two halves of the different phases. While the 2×2 reconstruction

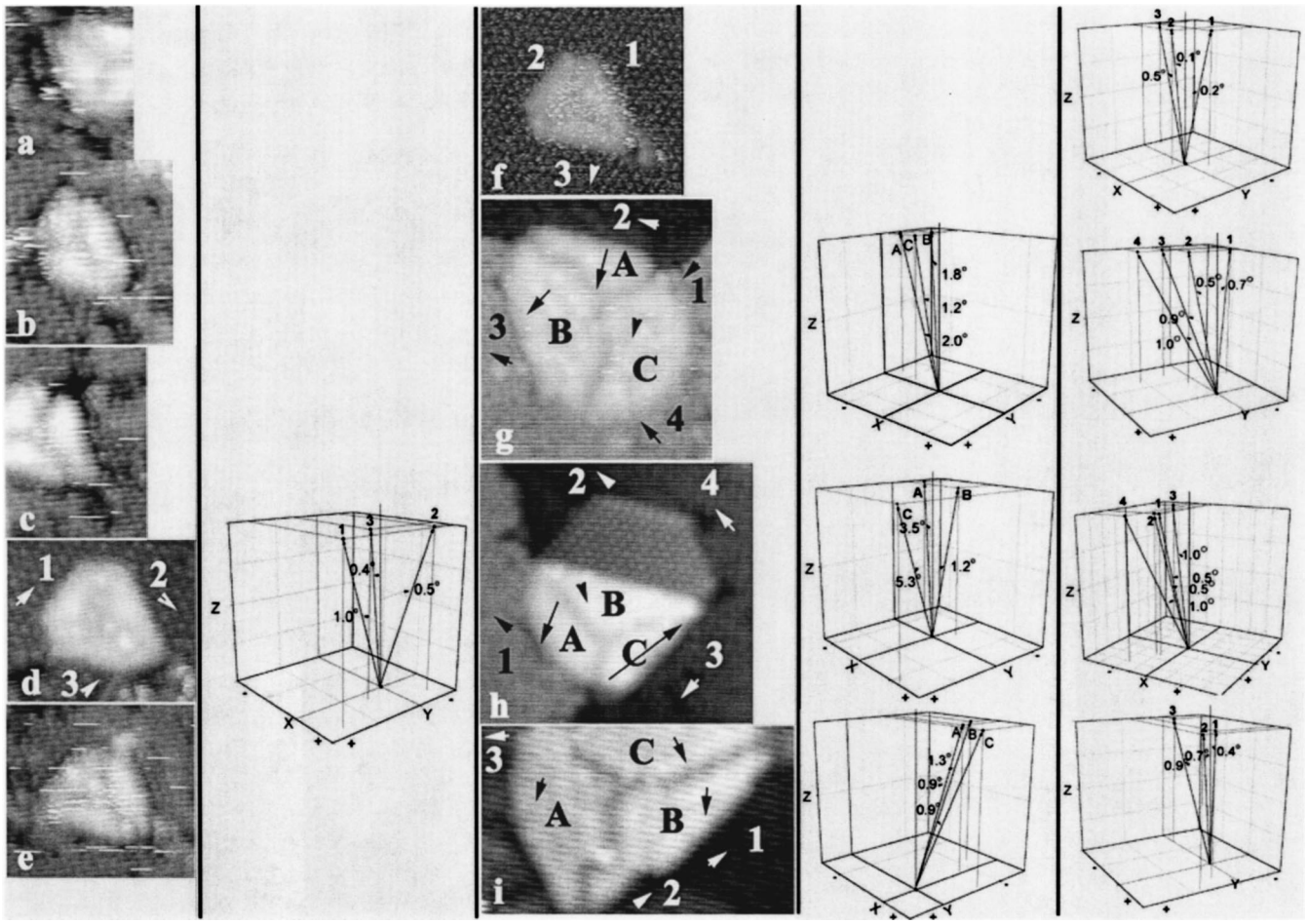

FIG. 3. Several β-$FeSi_2$ islands with different sizes. The islands are characterized by triangular shape with three trenches in the middle. All the images are in scale. The size of image h is 19 nm^2. The islands in a−i are with approximately 25, 22, 22, 25, 25, 22, 47, 30, and 52 atoms along the edge, respectively. $V_b = 2$ V and $I_t = 2$ nA. The deformations in each island are characterized in terms of the angles between the planes (characterized by letters inside and by number around the islands) and the surface normals. A three-dimensional plot of the vectors of the surface normals are presented to the right of each image. For clarity, the projection of these surface normals on the x-y plane are drawn on the image as arrows.

in the upper half is characteristic to the γ-$FeSi_2$ phase, the lower half does not have atomic resolution. In a previous paper we could identify the structure of the later phase by employing a Fourier transform to this part of the image and comparing it with the Fourier transform of the 2×2 part. It was concluded that this structure represents the β-$FeSi_2$.[10–12] No atomic resolution is noticed in real space in the β-$FeSi_2$ part of the island, but it is possible to see three prolonged depressions extending from the center of this part to its edges. Similar depressions appear in many other islands (e.g., Figs. 3 and 4) and are characteristics to the small β-$FeSi_2$ islands.

The depressions in the center of the β-$FeSi_2$ island are very shallow and wide. We characterized their dimensions in terms of depth and FWHM (full width at half maximum). These quantities are given for each cross section perpendicular to the depression. Such cross sections are drawn in Fig. 2 and marked by numbers. The dimension of the depressions is given in Table I (in Å). While these dimensions may not be precise and also vary from island to island, they represent the typical depressions. The depression lines are not fully symmetric, the angles between them are (in the majority of the cases) 110°, 140°, 110° (not 120°, 120°, 120°). We believe that these are the true angles but the possibility that this asymmetry is due to different scan velocities in the X and the Y directions cannot be excluded.

In smaller islands the size of the depressions is comparable with that of the island itself, suggesting that they are due to a continuous deformation of the island surface [Fig. 5(a)]. In contrast, the depressions in the larger islands are more localized in the center of the islands, are steeper [Fig. 5(b)], and may be considered as ''trenches.'' The effect of the depression localization can be seen in Figs. 3 and 4: the depressions are delocalized in the small islands [Figs. 3(a)–(f)].

The localization of the depressions into trenches in a large island indicates the development of line defects that separate three domains with different orientation due to the breaking of the degenerated crystallographic symmetry [Fig. 1(c)].

The uniform (small) island is deformed due to its mismatch. Breaking the island into three domains involves the release of the deformation energy at the cost of the line

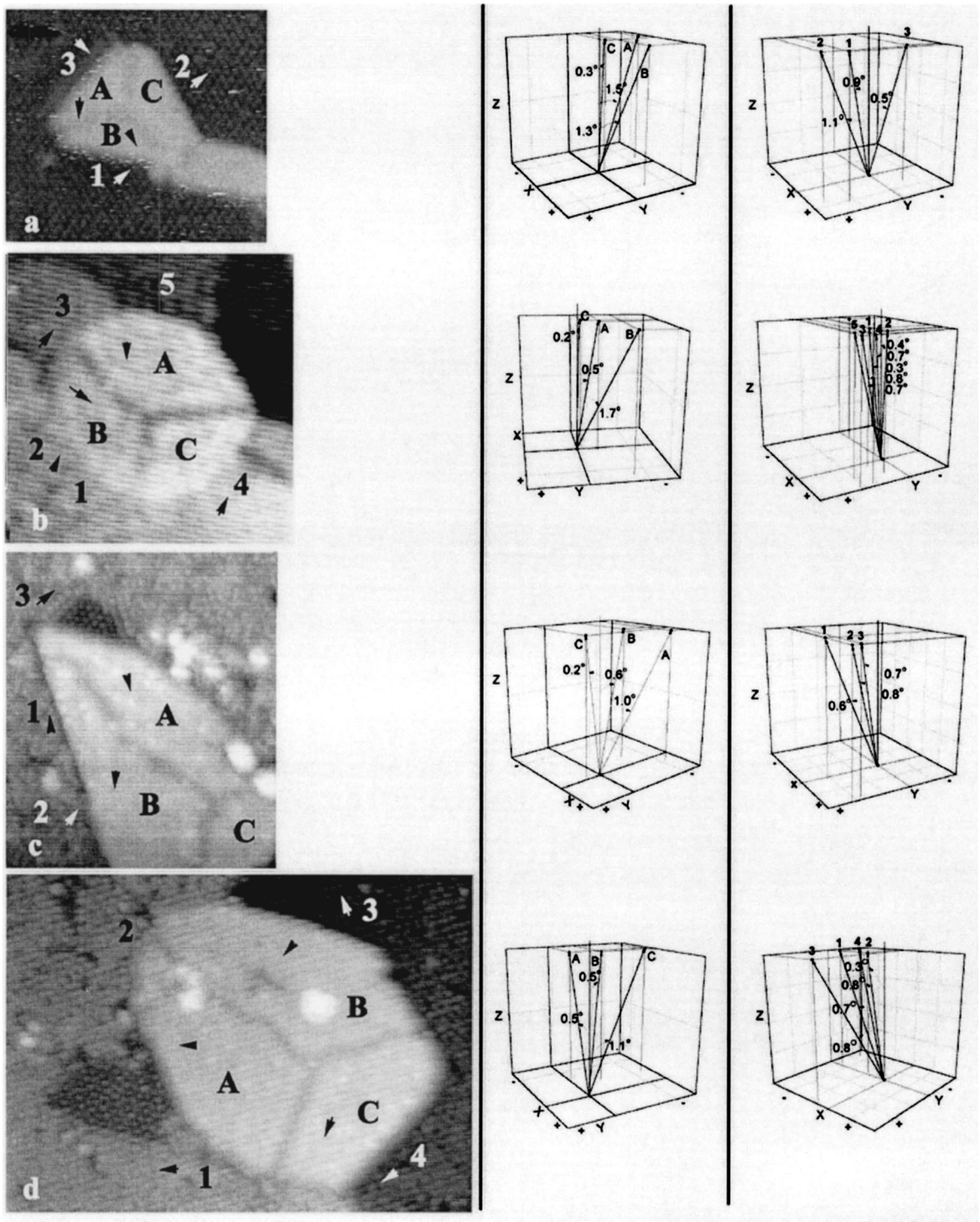

FIG. 4. Several larger β-$FeSi_2$ islands. The images are in scale. The size of the largest is $27\times38\ nm^2$. The islands at a-d are with approximately 33, 48, 57, and 77 atoms along the edge, respectively. The deformations are plotted in a similar form to Fig. 3. $V_b=2$ V and $I_t=2$ nA.

defect energy, and occurs at a critical island size. (Symmetry breaking is further discussed in the next section). Since the character of the line defect is yet unclear, we shall limit our elastic analysis to the *small* islands—below the critical size (delocalized depression).

In order to characterize the elastic interaction and to relate it to the observed structure, we found it useful to characterize the morphology of the island by three vectors that account for the average inclination of the surface triangular segment between each pair of depression lines. For this purpose, the angle between the segment average normal direction and the direction of the normal to the substrate surface was calculated. The normal to the surface was calculated for many points of each segment by computing the cross product

TABLE I.

	Left depression		Central Depression		Right Depression	
	Depth	FWHM	Depth	FWHM	Depth	FWHM
1	0.92	10	1.55	15	1.61	12
2	1.674	10	1.302	11	1.77	12
3	0.868	10	1.86	11	1.18	7
4	1.52	12				

between two vectors tangential to the surface at the point, thereafter averaged for the segment as a whole. The deviation of the segment inclination (e.g., the vectors indicated by A, B, C in Figs. 3 and 4) from the substrate normal varies from 1° to 5°. It was also found that the substrate area adjacent to the islands (designated by numbers 1, 2, 3, 4, 5 in Figs. 3 and 4) are not completely parallel to the surface. At this point we should point out that similar tilts or deformations are observed neither on the clean silicon 7×7 reconstruction nor on or around the γ-$FeSi_2$ islands.

The deformation of the islands on the free surface can be attributed to two factors: the misfit between the lattices of the island and the substrate and the surface stress of the substrate, which has a particular effect at discontinuities at the surface (like steps). In the following, we explore the source of the deformation.

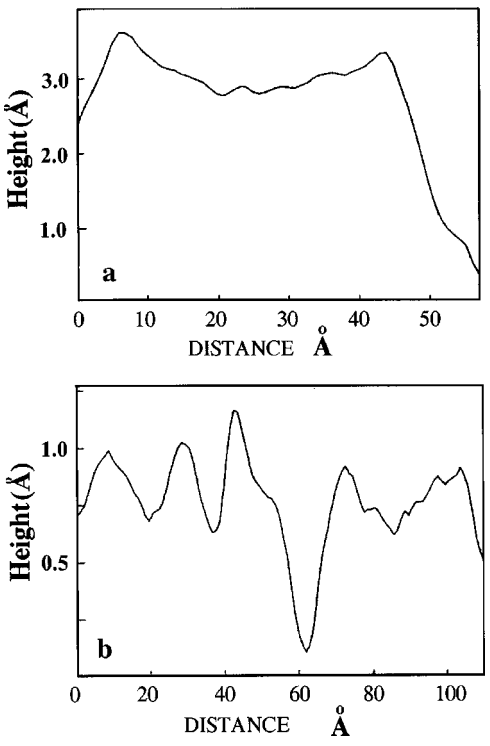

FIG. 5. Typical line scans from STM images of islands, demonstrating the shallow nature of the trench in smaller islands and the localization of the depression in the larger islands (a) small island [Fig. 3(d)] and (b) large island [Fig. 4(c)]. $V_b=2$ V and $I_t=2$ nA.

ELASTIC DEFORMATION OF SMALL ISLANDS

The crystallographic relation between Si(111) and β-$FeSi_2$ is threefold degenerated as shown in Fig. 1(a). The interatomic spacing of the silicide is shorter than that of silicon by 5.3% along the $FeSi_2[10\bar{1}]\|Si[\bar{1}\bar{1}2]$axis and longer by 1.4% along the $FeSi_2[010]\|Si[\bar{1}10]$axis.[4,8] Therefore, compared to its stress-free state, a small epitaxial silicide island is expected to be stretched along $FeSi_2[10\bar{1}]$ and compressed along $FeSi_2[010]$. The stress balance at the island and its vicinity was approximated within the framework of linear elasticity. The finite element (FE) method was used in order to solve the elastic boundary condition problem of the island-substrate interaction. This was done by using the NASTRAN™ code.[13] Our model consists of equilateral triangular island on a ten times larger triangular prism with free faces, as shown in Fig. 1(a).

The misfit between the island and the substrate was represented by two-dimensional (2D) thermal expansion that generates misfit stresses.[5] The contracted crystallographic axis $FeSi_2[10\bar{1}]$ is taken along the x direction with $\alpha_x\Delta T=-0.053$ (α is the thermal-expansion coefficient) and the dilated crystallographic axis $FeSi_2[010]$ is taken along the y direction with $\alpha_y\Delta T=0.014$. Throughout the calculations, the elastic constants of silicon ($C_{11}=165.7$, $C_{12}=63.9$, $C_{44}=79.56$ GPa Ref. 14) were transformed to the above system of coordinates of the silicon surface. For the $FeSi_2$ we used the Young modulus of 205 GPa, and a Poisson ratio of 0.23 (Ref. 15) (assuming isotropy in the absence of any other information). The surface stress was also simulated as thermal stress set up in the surface layer of the substrate surrounding the island, the thickness of which equals the height of the island. The magnitude of the surface stress is 2.37 eV/1×1 cell (1.25 N/m) in 7×7 reconstructed Si(111).[15] By and large, it was found that the effect of the substrate surface stress is to flatten slightly the island and it has a negligible effect on the orientation of the surface normals.

The island height uses the characteristic length of the model, i.e., the linear dimensions are scaled with this quantity. For instance, the ratio between the island edge length to its height determines uniquely the elastic fields distribution. When this ratio is 20, the scaling properties of linear elasticity means that the model represents an island of about 20 atoms along the edge in the case of a monolayer island. Figure 6 demonstrates the dependence of u_z, the calculated displacements in the direction normal to the substrate surface

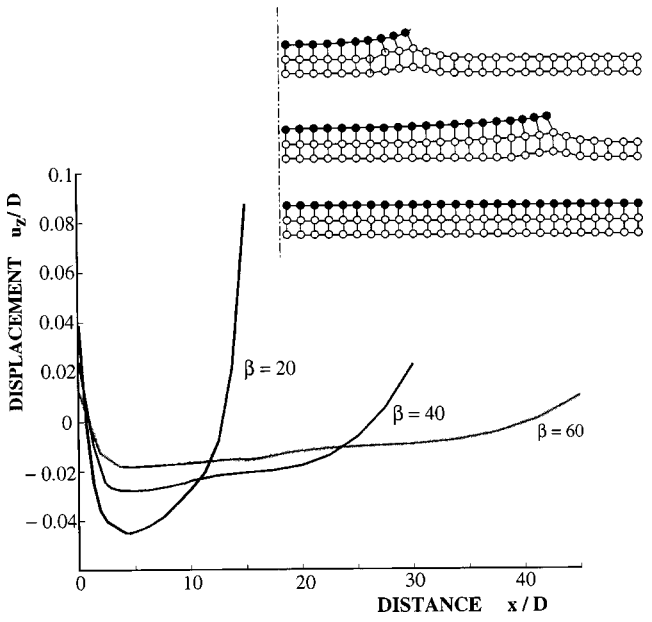

FIG. 6. Calculated displacements in the *z* direction of single-domain islands of three sizes: $\beta=20$, 40, and 60 atoms. The displacement is scaled with the island height. *D* is the diameter of an atom or the height of the island.

on the island size. The interaction with the substrate causes the tilting of the island, raising the island surface along its edge. It is seen that the degree of tilting decreases with the island size. This result fits the experimental observations that demonstrate *larger* tilt of the surface normals in the *smaller* islands (compare Fig. 3 to Fig. 4). It is clear that in the case of an infinitely extended epitaxial $FeSi_2$ layer, the constraint due to the silicon substrate periodicity imposes the maximum possible stresses in the layer (these stresses are given by substituting the minus misfit strains in Hook's law, $\sigma_{xx}=13.2$ GPa, $\sigma_{yy}=-0.3$ GPa). Under these constraints the monolayer would remain parallel to the substrate. However, in a *finite*-size island, stress relaxation occurs and causes the island to tilt. In each island the relaxation is confined to its periphery where the lateral forces are imbalanced. With increasing size of the island, the fraction of the peripheral atoms decreases and the tilt angle of the normals to the triangular decreases. In the following calculations, the model represents a monolayer island with 20 atoms along the triangular edge. Hence the calculated island is of the order of size of the islands in Figs. 3(a)–(f) and smaller than the islands in Figs. 3(g)–(i) and 4.

We first calculate the deformation of a triangular island with one of the possible orientations with respect to the substrate [Fig. 1(c)]. It is seen that bowing of the island along the *y* axis occurs, due to the contraction along the perpendicular *x* axis [Fig. 7(a)]. This result may explain the observation of the small islands, nonetheless it does *not* agree with the experimentally observed threefold mode of deformation. Hence we refine the model by breaking the internal symmetry of the island, based on the following observations. Raunau *et al.*[10] noticed that β-$FeSi_2$ grows epitaxialy on (7×7) surface in *three* equivalent orientations that are mutually rotated by 120°. These relations are shown in Fig. 1(c). In view of the observation that the large islands contain three line defects dividing each island to three approximately equal triangular areas, we employed the Raunau *et al.* argument and conjecture that each subarea is one of the three crystallographicaly equivalent domains, and that the observed line defects are the domain boundaries. The proposed atomic arrangement at the node between the three domains is shown in Fig. 1(c). The idea is that the nearly triangular shape of the island and its domains are not accidental: it makes possible to orient the high-strain axis along the *short* dimension of each triangular domain (its short height) thus to avoid the large elastic strain. In contrast to the large island, the distortion in the small island is not localized to the line defects, but extends symmetrically throughout the island.

To realize this state of external forces, the FE model was revised in order to simulate the resulting strain field and morphology. The equilateral triangular island is subdivided into three equal triangle segments. The -5.3% strain and the $+1.4\%$ strain is applied to it as shown in Fig. 1. The matching condition at the segments boundaries assumed continuity of the three components of the displacement. It should be reemphasized that this condition adequately represent the case of a small island, where the depression is delocalized, and the line defect has not been formed. The obtained displacements along the *z* axis are shown in Fig. 7(b). A symmetric folding is immediately observed with symmetric threefold depression at the center of the island. Qualitatively, this result agrees with the experimental observed morphology. Fig. 7(d) presents the deformation of an equilateral triangular island with nonequilateral domains under the same condition of the mismatch strain. The tilt angles of the surface normals in the smaller domain are larger. This is in agreement with the experimental observations.

The next factor to be taken into consideration is the surface stress, which was determined to be 2.37 eV/1×1 cell (1.25 N/m) in 7×7 reconstructed Si (111).[16] The surface stress is also simulated as thermal stress set up in a layer in the substrate surface surrounding the island. It is taken to prevail in the surface layer with thickness equivalent to two atomic layers. The resulting deformation is depicted in Figs. 7(c) and (e). The tensile surface stress slightly flattens the island but have negligible effect on the orientation of the surface normals. The rotations of these normals are in the range of the observed angles, and are nonsensitive to the magnitude of the surface stress.

An abundant observation in STM images is the heterogeneous nucleation of islands at the vicinity of surface steps. In these cases it is commonly observed that the islands lie partly on the upper terrace and partly on the lower terrace. We observed islands adjacent to steps that we presume consisting of a bilayer on the lower terrace and a monolayer at the upper terrace, as shown in Fig. 1(b). In all cases the measured surface normals were inclined toward the upper terrace of the step. The elastic interaction at the step is not trivial and should be dominated by the (linear) force exerted at the step contour, normal to the step, which replaces the dipole interaction of the bared step.[17] Three FE models were prepared to simulate islands that cover steps to different degrees. The resulting deformations are shown in Figs. 8(a)–

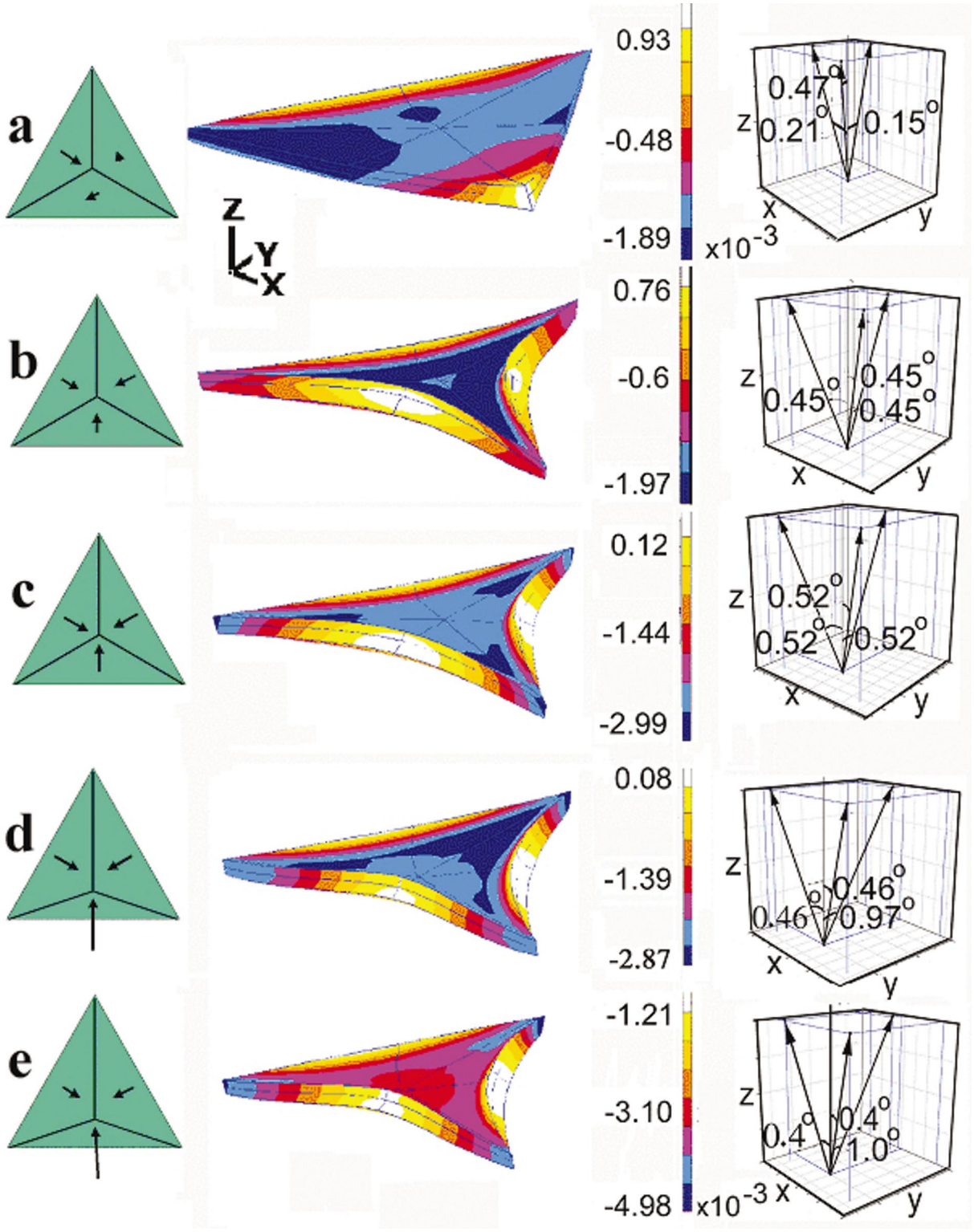

FIG. 7. (Color) (a) Finite element calculation for a triangular β-$FeSi_2$ island on a substrate of (111) silicon. The shapes of the triangles simulate the shape of the deformed islands, the color fringes are scaled according to the u_z component. A deep trench is apparent in the y direction corresponding to the $[1\bar{1}2]$ direction in the images. The calculations were made for aspect ratio of 20, representing the number of atoms along each edge. (b) The island is combined of three domains with their β-$FeSi_2$ [101] axes parallel to the short height of each domain. Three intersecting trenches are apparent. (c) The three-domain island with 1.25 N/m surface stress on the substrate surface, (d) and (e) two nonsymmetrical islands, without and with surface stress, respectively. The displacement is scaled with the island height.

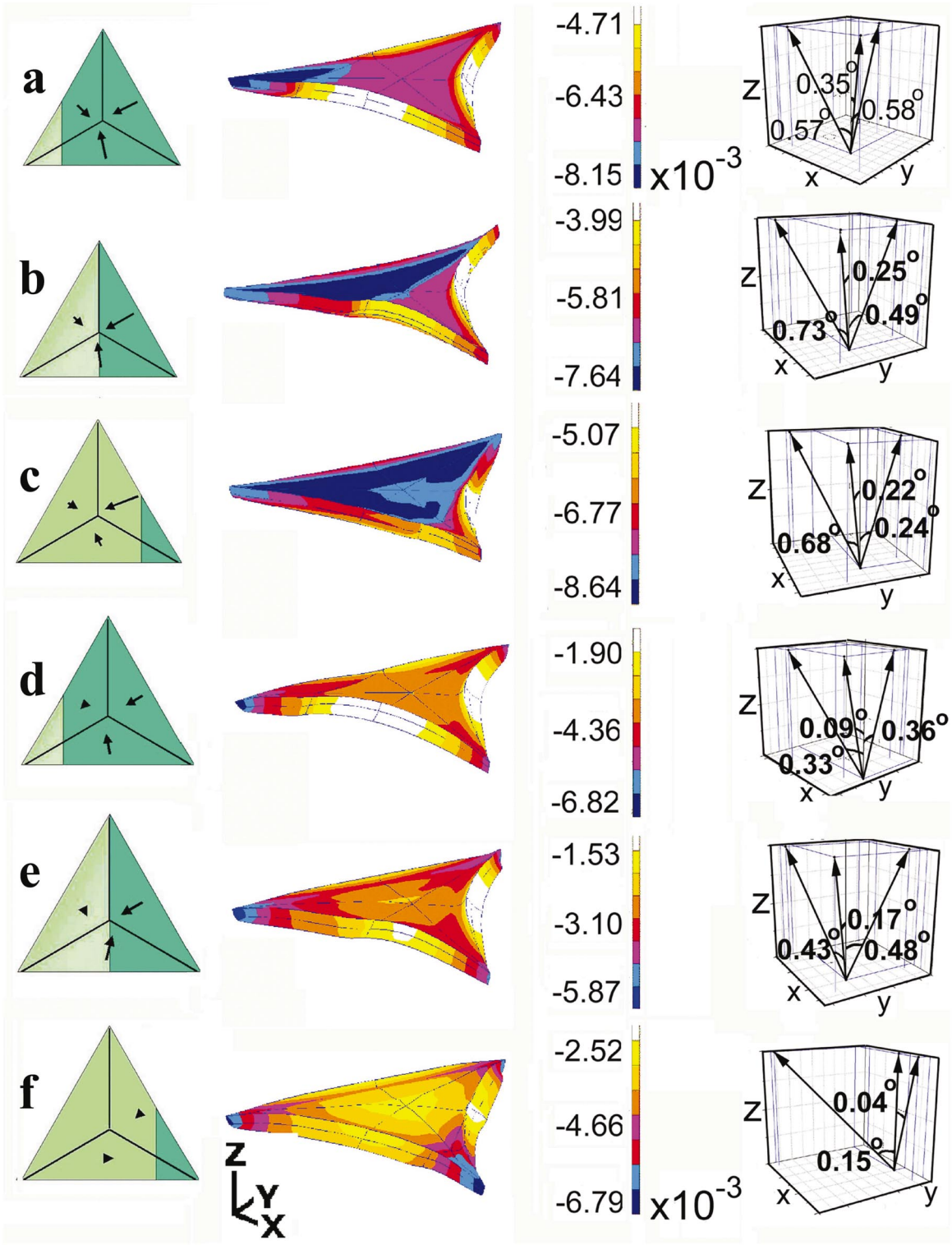

FIG. 8. (Color) Calculated deformation of island adjacent to surface *steps* [Fig. 1(b)]. (a)–(c). Three different locations of the islands relative to the step. The tensile surface stress is assumed continuous in the substrate layer of two atom thickness, (d)–(f). The same locations of the islands relative to the step, but tensile surface stress exists now only on the free surface of the substrate. The color fringes represent the u_z component. The displacement is scaled with the island height.

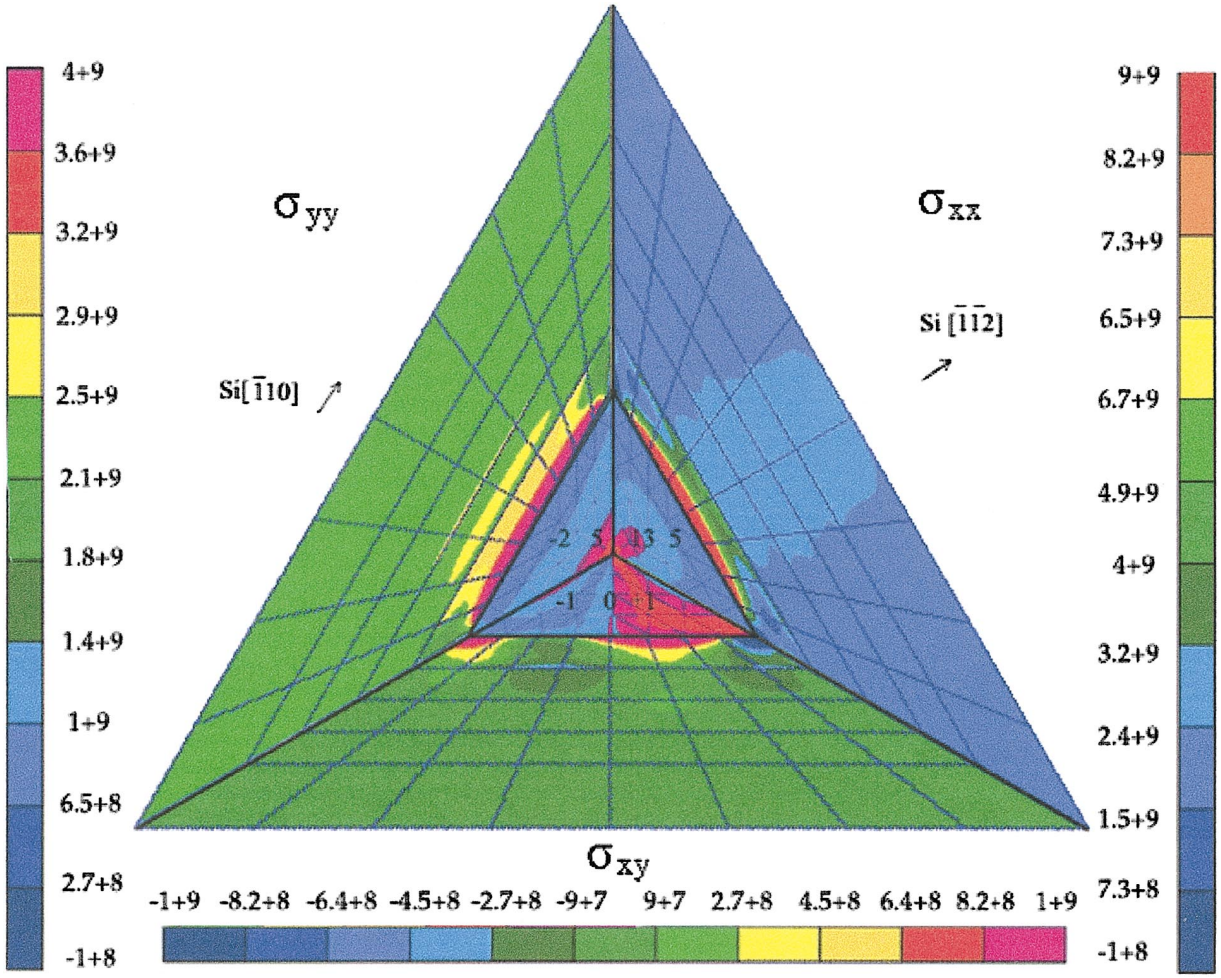

FIG. 9. (Color) A mosaic of the calculated stresses in the vicinity of a three-domain island: in the right-hand triangle the stress σ_{xx} is plotted, in the left-hand triangle the stress σ_{yy} is plotted, and in the lower triangle the shear stress σ_{xy} is shown. Three scales are applied for each stress component, they are expressed in [Pa]. The stresses in the island are plotted in scales different from those on the substrate. The scales in the island are indicated by numbers on the fringe boundaries standing for the stress there in GPa. The stress far from the island converge to the surface stress on Si(111), which is equivalent to 2.2 GPa in the present model.

(c). In agreement with the experiments, the inclination of the domain normals toward the steps increased. Since the experiments provide exact values of the normal orientation, interesting local elastic properties of the surface may be learned. As an illustration, we compare two representations of the surface stress on silicon. The first assumes that it is continuous even below the island. Figures 8(a)–(c) are the results for this case. The second assumes that the surface stress of Si(111) is interrupted below the island which implies that the surface under the islands is converted into the unreconstructed structure. The results for this case are shown in Figs. 8(d)–(f). The surface normal inclinations are larger in the first case. Nevertheless in both cases the calculated tilt angles were always smaller than the measured ones. This discrepancy might be explained by the presence of defects in the large islands, and the arbitrary choice of the intermediate phase and representation of the surface stress.

Once a model of the stress source is assessed, one can calculate the elastic fields it generates at long distances on the substrate surface. This extension of the approach is shown in Fig. 9, where the elastic stresses are shown in a triangle surrounding a $FeSi_2$ island. The figure is a mosaic of three contour maps: in the right hand triangle the stress σ_{xx} is plotted, where x is the Si$[\bar{1}\bar{1}2]$ crystallographic direction, in the left hand triangle the stress σ_{yy} is plotted, y is the Si$[\bar{1}10]$ crystallographic direction. In the lower triangle the shear stress σ_{xy} is shown. The stresses in the substrate are largest in front of the island edges. The effective range of the stresses is of the order of one edge of an island. σ_{xx} is about twice the magnitude of σ_{yy} and both are tensile. σ_{xy} has a twofold symmetry about the island centerline and is an order of magnitude smaller than the tensile stresses. At long distances from the island the stresses converge to bi-axial tension due to the surface stress.

The stresses transmitted on the surface are responsible for the elastic interactions between islands. A β-$FeSi_2$ island will be attracted by compressive stresses, hence we find that the $FeSi_2$ islands interact repulsively with each other. The stresses should of course be considered effective stresses in

these atomic scales. This research may point to the possibility to use the measured deformation as an input boundary condition to the calculation of the elastic fields.

DISCUSSION

The out-of-plane displacements measured by STM and accompanied by elastic calculations revealed the local deformations at the surfaces and the bulk. It is seen that the small triangular silcide islands are bowed on the silicon substrate to relieve mismatch stress. When the island grows, long wavelength stresses are localized into line defects that separate domains of broken symmetry with reduced stress. The calculations of the deformation in the substrate/small-island system agrees, at least qualitatively with the measured displacements, hence enables us to use the measurements in order to evaluate the elastic fields distribution in the system. The significance of such measurements may become evident from the following discussion of alternative approaches.

Attempts have been done to measure the mechanical properties near the surface. This includes: (i) nanoindentation[17,18] is a widely used method to determine the elastic properties of the surface of very thin films. In this technique, a diamond indenter is pressed into the sample. The force that pushes the indenter into the sample is increased continuously (loading mode). After a certain penetration depth, the force is reduced and the elastic response of the sample pushes the indenter outside the surface (unloading mode). The slope of the force displacement curves during unloading is related to the Young modulus. The advantage of the nanoindentation technique is that it is possible to measure the elastic constants with high precision (together with parameters that characterize the plastic and fracture behavior of this sample). The disadvantage is that the resolution is quite limited and that the method is invasive and the sample is modified. (ii) The bending beam method[19–21] provides high accuracy but without spatial resolution. The idea is to cover a flexible cantilever by a thin film. If the film has some surface stress, it will bend the cantilever. The radius of curvature of the bending is related to the film stress. The bending of the cantilever is measured by optical means or by capacitance. The Young modulus, the Poisson ratio, and the coefficient of thermal expansion of the thin film were measured simultaneously when deposited both on isotropic and anisotropic substrate.[22] The stress induced by adsorbates, reconstructions, etc., was measured with high precision with this technique,[6] demonstrating the rich information that might be obtained by the method. (iii) Atomic force microscopy[23] is expected to measure local mechanical properties with high accuracy and high lateral resolution. In practice, it is difficult to isolate the parameters related to elasticity, from those related to adhesion, friction, dissipation, and damping, etc. Many techniques were developed to achieve nanometric scale profiling of the mechanical properties: In the force modulation atomic force microscopy (AFM) techniques,[24] the elastic properties of the substrate change the contact stiffness and can be therefore measured. In the tapping mode, the phase contrast of the AFM can be related to the elastic properties in some cases;[25] additional possibilities are to measure shifts in the cantilever resonance frequencies as a result of the contact stiffness.[26] A ''hybrid'' nanoindenter[27] claims an accuracy of 20% in moduli measurements. (iv) Ultrasonic force microscopy is done by modulating the position of the tip at high frequencies.[28] It is possible to use the nonlinearity of the force/distance curve, in order to observe a dc shift of the force. It was shown that such a measurement could provide local measurements of the mechanical properties and the elastic strain. However, it is difficult to isolate the strain effect from other mechanical and morphological factors, hence the local strain could not be quantify at this stage.

These techniques successfully measured the mechanical properties near the surface. However, as far as the lateral force distribution and the in-depth profiling of the strain field are concerned, they have not been attempted to provide answers. The present approach complements these techniques by providing the local surface mechanical properties at a nanometric scale, both in the lateral and vertical directions. Based on this approach, an iterative algorithm may be developed in attempt to fit the mechanical properties on the nanometric scale of the surface. Then, the technique may be extended to provide full account of the elastic field distribution on the surface, as done in Fig. 9.

In spite of the success in this first demonstration of the method, it should be recalled that some of the details could not be explained in our work: the experimentally observed rotation angles of the free islands and the island at the vicinity of steps are larger than the calculated one. The discrepancy calls for refinements. Effort should be dedicated towards the understanding the structure of the line defects in the large island, and accordingly to redefine the boundary conditions for the elastic problem. Next nonlinear elasticity may be applied.

We discussed the elastic induced deformations, assuming that no plastic deformation of the surface took place. Of course, if the level of strain exceeds the elastic limit, the surface will be plastically deformed. It has been demonstrated that such deformations can also be discerned with STM.[29]

In conclusion, it is shown that elastic stress field of the island (or other nanometric features) on the surface can be determined by combining the out-of-plane STM measurements of local displacements with the available computation. Further extension of this approach may yield additional information about the mechanical properties at the surface in the nm scale.

ACKNOWLEDGMENTS

The experimental work was supported by the German Israeli Binational Foundation for Research and Development (GIF). Additional support was given by grants from the Israel Science Foundation (ISF).

[1] G. Khachaturyan, *Theory of Structural Transformations in Solids* (Wiley, New York, 1983).
[2] J. E. Hilliard, in *Phase Transformations* (ASM, Metals Park, OH, 1968), Chap. 12.
[3] R. Z. Shneck, Philos. Mag. A **81**, 383 (2001).
[4] J. P. Hirth and J. Lothe, *Dislocations in Solids* (McGraw Hill, New York, 1968).
[5] D. Bimberg, M. Grundmann, and N. N. Ledentsor, *Quantum Heterostrctures* (Wiley, Chichester, 1999), Chaps. 4 and 5.
[6] H. Ibach, Surf. Sci. Rep. **29**, 193 (1997).
[7] O. V. Kolosov, M. R. Castell, C. D. Marsh, G. A. D. Briggs, T. Kamins, and R. S. Williams, Phys. Rev. Lett. **81**, 1046 (1998).
[8] A. L. Vazquez de Parga, J. de la Figuera, O. Ocal, and R. Miranda, Europhys. Lett. **18**, 595 (1992).
[9] H. von Känel, K. A. Mäder, E. Müller, N. Onda, and H. Sirringhaus, Phys. Rev. B **45**, 13 807 (1992).
[10] W. Raunau, H. Niehus, T. Schilling, and G. Comsa, Surf. Sci. **286**, 203 (1993).
[11] N. E. Christensen, Phys. Rev. B **42**, 7148 (1990).
[12] Y. Manassen, I. Mukhopadhyay, and N. Ramesh Rao, Phys. Rev. B **61**, 16 223 (2000).
[13] MSC/NASTRAN, The MacNeal-Schwendler Corporation, LA.
[14] Landolt-Bŏrnstein, New Series, Group III, Vol. 1, Pt. 1, edited by K. H. Hellwege and A. M. Helwege (Springer-Verlag, Berlin, 1979).
[15] *Metal Silicides*, EMIS Datareviews Series No. 14, edited by Marc Van Rossum (INSPEC, London, 1995), p. 24.
[16] R. E. Martinez, W. M. Augustyniak, and J. A. Golovchenko, Phys. Rev. Lett. **64**, 1035 (1990).
[17] V. I. Marchenko and A. Ya. Parshin, [Zh. Eksp. Teor. Fiz. **79**, 257 (1980).
[18] M. F. Doerner and W. D. Nix, J. Mater. Res. **1**, 601 (1986).
[19] W. C. Oliver and G. M. Pharr, J. Mater. Res. **7**, 1564 (1992).
[20] A. Schell-Sorokin and R. M. Tromp, Phys. Rev. Lett. **64**, 1039 (1990).
[21] D. Sander and H. Ibach, Phys. Rev. B **43**, 4263 (1991).
[22] H. Ibach, C. E. Bach, M. Giesen, and A. Grossmann, Surf. Sci. **375**, 107 (1997).
[23] J.-H. Zhao, Y. Du, M. Morgen, and P. S. Ho, J. Appl. Phys. **87**, 1575 (2000).
[24] G. Binnig, C. F. Quate, and C. Gerber, Phys. Rev. Lett. **56**, 930 (1986).
[25] E. L. Florin, M. Radmacher, B. Fleck, and H. E. Gaub, Rev. Sci. Instrum. **65**, 639 (1994).
[26] J. Tamayo and R. Garcia, Appl. Phys. Lett. **71**, 2394 (1997).
[27] S. Amelio, A. V. Goldabe, U. Rabe, V. Scherer, B. Bhushan, and W. Arnold, Thin Solid Films **392**, 75 (2001).
[28] S. A. Syed Asif, K. J. Wahl, R. J. Colton, and O. L. Warren, J. Appl. Phys. **90**, 1192 (2001).
[29] A. Pundt, M. Getzlaff, M. Bode, R. Kirchheim, and R. Wiesendanger, Phys. Rev. B **61**, 9964 (2000).